OPTIMAL SEISMIC PHASES FOR FULL-WAVEFORM INVERSION OF GLOBAL DISCONTINUITIES USING SPECTRAL-ELEMENTS

Maria Carrizo Dr. Maria Koroni, ETH Zurich

August, 2019

Contents

1 Introduction **1**

2 Methodology **2**
2.1 Spectral-element simulations 2
2.2 Analysis of Synthetic Waveforms 3
2.2.1 Sensitivity of the P-wave to the Topography in the '410' and '660' discontinuities 3
2.2.2 Sensitivity of the S-wave to the Topography in the '410' and '660' discontinuities 5
2.3 Real Event Comparison with Synthetic Experiment 9
2.3.1 Traveltime difference 9

3 Results **10**

4 Discussion **13**

5 Conclusions **17**

6 Recommendations **18**

References **18**

A Appendix 1 **20**

Abstract

Using the spectral-element modelling method we investigated the effect of topography in the upper mantle discontinuities on the traveltimes of seismic phases in both shear and compressional wave, including SS and PP precursors, as well as ScS and PcP core reverberations. We simulated exact seismograms in 1D and 3D elastic models of the mantle. In a second simulation, we added topography to the discontinuities. We compared the waveforms obtained with and without topography by obtaining amplitude direct difference for a window enclosing each seismic phase evaluated. Based on the resulting values of amplitude direct difference we proposed a classification of seismic phases sensitivity to the topography in the upper mantle discontinuities. To further evaluate the sensitivity of the seismic phases to the topography in the upper mantle discontinuities we compared seismograms resulting from a real event to simulated seismograms in 1D and 3D elastic models of the mantle. We studied the cross-correlation traveltime difference between the real and synthetic seismograms in a 50 seconds window using a quality control of maximum $\pm$ 20 seconds time shift for each seismic phase arrival. The resulting traveltime values are presented in histograms, which indicate a similar sensitivity behaviour of the seismic phases to topography in the upper mantle discontinuities.

1 Introduction

Earth's mantle plays an important role in the planet dynamics and provides the thermal and mechanical driving forces for plate tectonics. Heat liberated by the core is transferred into the mantle where most of it is convected through the mantle to the base of the lithosphere. The remainder may be transferred upward by mantle plumes generated in the coremantle boundary layer. The mantle is also the destination for descending lithospheric slabs, and the evolution of these slabs in the mantle is the subject of ongoing discussion and controversy. Thus, further studying and constraining the structure of the mantle layers is imperative to solve these hypotheses.

The upper mantle discontinuities imaging through seismic data is very useful to provide necessary information to constrain models of mantle mineral composition and pressure-temperature dynamics. The analysis of seismic evidence of discontinuities in the upper mantle began over 50 years ago with the increasing abundance of seismological data worldwide [Shearer, 1991].

Discontinuities near 410 and 660 km depth (also named as upper mantle discontinuities) are now a standard feature in mantle models, based on detailed traveltime and synthetic seismogram analyses of both compressional and shear waves. The mantle discontinuities at 410 and 660 km form the upper and lower bounds of a layer of the mantle known as the mantle transition zone (MTZ), that separates the upper mantle zone from the lower mantle zone [Vinnik, 2011]. Each zone is characterised by different mineral composition and properties, which translates to changes in the behaviour of the seismic waves.

The 410 km depth discontinuity is interpreted as the transition from olivine (Mg_2SiO_4) to its polymorph β-olivine (Wadsleyite) [Helffrich, 2000]. This transition occurs at a temperature of about 1400-1450°C. The P- and S-velocity contrasts at the discontinuity are around 0.5 km/s and $0.2 - 0.3$ km/s, respectively. The Clapeyron slope of this transition is positive 4.0 MPa/K; the increase of the S-wave velocity is $\sim 12\%$. An accurate determination of this thickness is, however, difficult. The published estimates vary between 0 km and 100 km partly due to ambiguity of data and partly due to lateral variations of sharpness of the discontinuity [Katsura et al., 2004]. The observations of the phases converted from P to S at the 400 km depth imply that the thickness of the discontinuity is less than $30-$ 50 km.

The 660 km depth discontinuity is interpreted as the transition from γ-olivine to perovskite ($MgSiO_3$), with a temperature estimate of about 1,600C. The S velocity contrast of this transition is comparable to that of the α/β transition. The transition is sharp and has a negative Clapeyron slope of -2.8 MPa/K [Hirose, 2002]. These discontinuities can have variations of ± 20 km depending on temperature and composition, and possibly with variations more than twice as large for narrow areas inside hot plumes and cold slabs [Deuss, 2009]. These topographic variations are a physical representation of dynamic processes of the earth that geoscientists aim to constrain and understand.

The systematic investigation of the topography of the discontinuities at 410 and 660 km depth through seismological data has been conducted in many previous studies with a variety of techniques, mainly with the use of precursors of surface reflected phases SS and PP [Shearer, 1991, Vasco and Johnson, 1998], other phases of interest include P and SH multiples resulting from topside reflections [Ward, 1978, Deuss, 2009, C. Schmerr et al., 2010] and P-to-S converted phases [Vinnik, 1977, Cottaar and Deuss, 2015].

In this research we used spectral-element forward modelling of the seismic wavefield to obtain synthetic seismograms that will be used to investigate the effect in the waveforms of the variation in topography of the upper mantle discontinuities at 410 and 660 km depth and identify which seismic phases are related to these effects. The seismograms with and without topography are compared by calculating amplitude direct difference for windows enclosing the seismic phases evaluated for shear and compressional wave. Afterwards, we consider a classification of seismic phases sensitivity in a qualitative manner by observing the results of amplitude direct difference curves.

In order to further evaluate the seismic phases sensitivity to topography in the upper mantle discontinuities we performed a comparison of a real event with spectral-element method, using cross-correlation, obtaining traveltime difference histograms for each seismic phase evaluated. The sensitivity of the shear wave seismic phases shows a similar response to the synthetic experiments.

2 Methodology

2.1 Spectral-element simulations

To study the sensitivity of certain seismic phases to the variations in topography of the 410 and 660 km discontinuities (from now on mentioned as '410' and '660') we take the advantage of using synthetic experiments to generate data through spectral-element modelling, using the code `SPECFEM3D_GLOBE`©, which simulates three-dimensional global and regional seismic wave propagation based upon the spectral-element method (SEM). It was developed by [Komatitsch and Vilotte, 1998, Komatitsch and Tromp, 1999, Komatitsch and Tromp, 2002b, Komatitsch and Tromp, 2002a].

We generated simulations of earthquakes that provides exact synthetic seismograms in 1D and 3D elas-

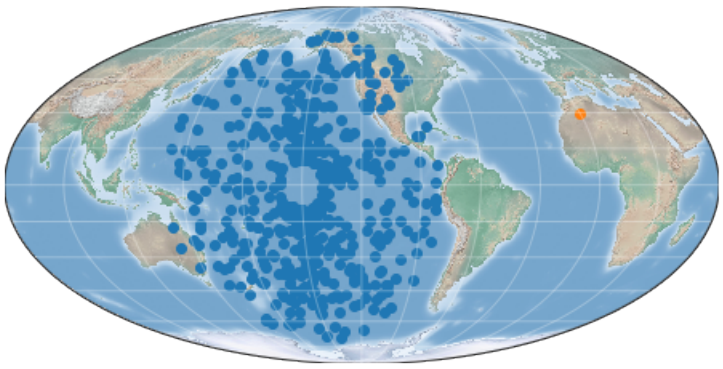

Figure 1: Stations for spectral-element simulations (blue dots) and location of event simulated (orange dot)

Magnitude	7.9
Latitude	0 N
Longitude	30 E
Source time function	Gaussian half-width 4 seconds
Depth	20 km

Table 1: Simulated Event Parameters

tic models of the mantle. The 1D elastic earth model simulations is based on the background model PREM [Dziewonski and Anderson, 1981]. The 3D elastic earth model simulations uses the background model S20RTS [Ritsema et al., 1999] combined with CRUST2.0 [Bassin et al., 2000]. Afterward, we analyzed the differences in the synthetic seismograms response to switching on or off the topography variations in the '410' and '660' discontinuities. The earth model the topography models used for the '410' and '660' discontinuities used were derived from [Meier et al., 2009], which contains lateral variations up to spherical harmonic degree ≤ 8. This evaluation was carried out by comparing traveltime arrivals of a group of body phases. The main goal is to determine whether the topography variations of the mantle discontinuities in the models results in shifts in the arrivals of the body phases, and to determine which body wave present more sensitivity to these variations. The added features for the code (attenuation, rotation, ellipticity, gravity and surface topography) were not included in these simulations.

It is important to note that we did not add noise to the seismograms. The stations were spread randomly creating a regular distribution of interactions with the '410' and '660' discontinuities inside an epicentral distance range of 110° to 170° to avoid interference by surface multiples or topside reflections. In each Earth model case one hour-long seismograms are created for 522 stations, which can be seen in the Figure 1. The parameters defined for the event simulated can be found in Table 1.

Using the Taup Toolkit©, developed by [Crotwell et al., 1999] we obtained the theoretical travel time arrivals used to identify the response of the seismic phase signal on the seismograms. We chose a group of seismic phases (compressional and shear wave) to be assessed in the study, given that these phases interact with the upper mantle for in a seismic event.

2.2 Analysis of Synthetic Waveforms

2.2.1 Sensitivity of the P-wave to the Topography in the '410' and '660' discontinuities

For the vertical component seismograms we selected the following group of seismic phases considering the fact that these interact with the mantle. The seismic phases evaluated for P-wave are: Pdiff, PKIKP, PKP, PKKP, PKIKKIKP, P660P, P410P, PcP660PcP, PcP410PcP, PP, PcPPcP, PP660P, PP410P, PPP, PcPPcPPcP and PPPP. The theoretical ray paths for these seismic phases are illustrated in Figure 2.

1D Elastic Model

In the simulation created for the 1D Elastic Model, vertical component traces were generated for the synthetic seismic stations. For these seismograms we evaluated amplitude variations for the P-wave seismic phases pre-

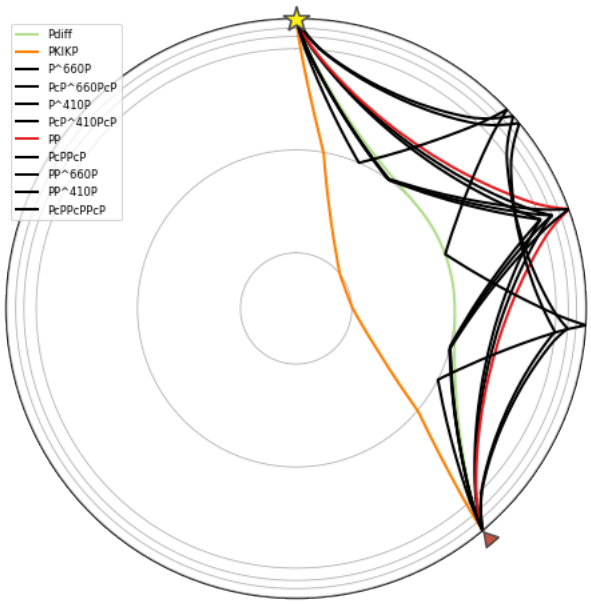

Figure 2: Raypaths of the Compressional Wave seismic phases investigated

viously mentioned. We evaluated the variations caused in the waveforms by adding the topography in the '410' and '660' discontinuities by calculating the direct difference between the two waveforms with and without the topography anomalies, using Equation 1.

$$\Delta 1D = 1D^{PREM} - 1D^{PREM+Topo} \tag{1}$$

In Figure 3 we can observe the seismograms pair resulting for the a station with epicentral distance 141.75° for the cases with and without topography and the events related to the phases PKIKP, PKP, P660P, P410P, and PP. In the seismograms plot we defined windows that enclose the response of the seismic phases, where we can visually identify which time windows contain variations with topography between the waveforms. The effect in amplitude variations for each phase arrival was evaluated for a 30 seconds window after the theoretical arrival using Equation 1. The results are shown in Table 2 in the column Δ1D.

Moreover, we also calculated direct difference curves between the seismograms pairs for all stations, presented in Figure 4. Marked in lines are the theoeretical arrivals of the P-wave seismic phases. It is possible to observe that for the seismic phases evaluated the theoretical traveltimes lines are followed by the events related with amplitude differences. The highest amplitudes are shown by the phases PcPPcP, PP, PPP and PPPP.

It is important to remember that for the calculation of the amplitude differences the seismograms were normalized. If we consider the true amplitudes of the seismograms resulting from the simulation we can see that the amplitudes of the vertical component are much smaller than the amplitudes of the transverse component, thus the amplitudes of the differences calculated will also have smaller values for the vertical component compared to the transverse component.

3D Elastic Model

We used the same methodology from the 1D cases where seismograms were generated, this time using the earth model S20RTS + CRUST2.0. Two cases were created: one case without topography in the '410' and '660' discontinuities and one case including topography in the '410' and '660' discontinuities.

For an example station we evaluated the variations caused in the waveforms by adding the topography in the '410' and '660' discontinuities by calculating the direct difference between the two waveforms, using Equation 2, in a 10 seconds window after the theoretical arrival traveltimes of the seismic phases evaluated for P-wave. The results are shown in Table 2 in the column Δ3D.

$$\Delta 3D = 3D^{S20RTS} - 3D^{S20RTS+Topo} \tag{2}$$

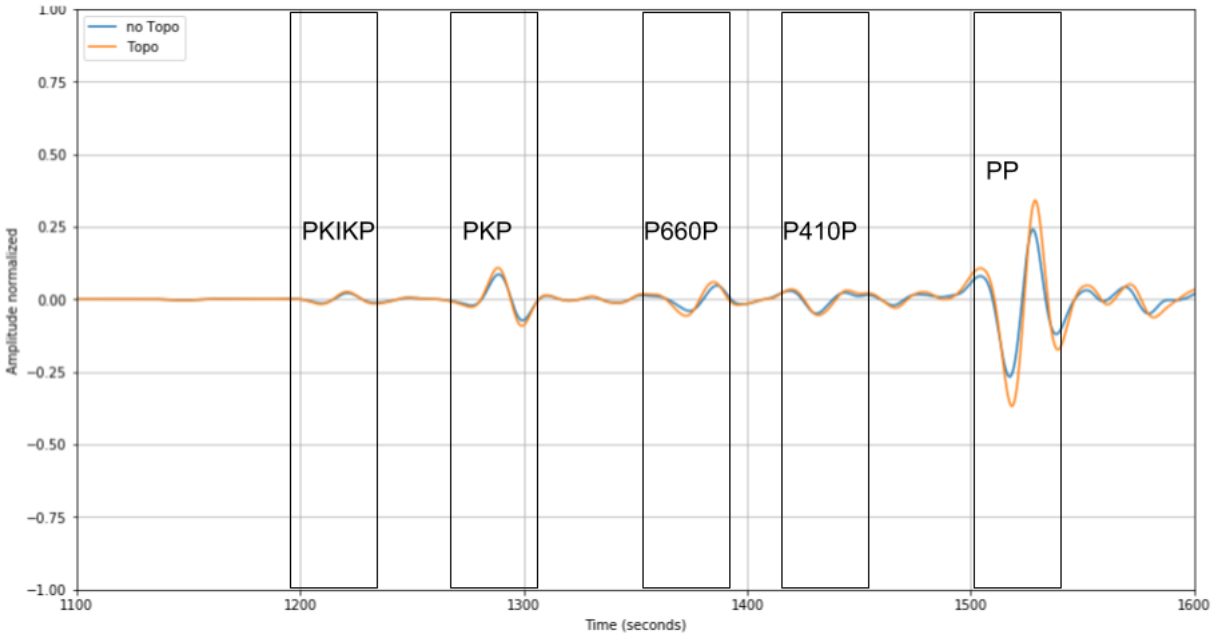

Figure 3: Vertical component seismograms for a station with epicentral distance 141.75° - 1D Elastic Model

We also calculated difference plots between the seismograms with and without topography for all stations. In Figure 5, curves are presented that plot the differences calculated with Equation 2 for all the stations used in the simulations for the 3D elastic earth model cases. Marked in lines are the theoeretical arrivals of the seismic phases. From Table 2 we can observe that the seismic phases sensitivity behaviour is similar for the simulations generated in both 1D elastic earth model and 3D elastic earth model.

Effect of event depth in P-wave seismic phases:

In order to further evaluate the parameters that control the synthetic data response to variations in the '410' and '660' discontinuities topography, we considered following the same methodology to generate the amplitude direct difference curves for three events with depths: 20 km, 150 km and 500 km. The goal was to investigate if the shallowest depth events could have be affected by surface waves and provide different results for the sensitivity analysis of the seismic phases.

We followed the same methodology of seismic phase sensitivity evaluation for the three events in all stations to obtain the direct differences for the seismic phases in both 1D elastic model and 3D elastic simulations. We obtained a very similar behaviour in seismic phase sensitivity according to the values of amplitude direct difference for the three different depth events. From this result we can infer that the depth of the event might not affect the results of phases sensitivity in the simulations. Consequently we have summarized in Table 3 a classification of the P-wave seismic phases in proportion to the sensitivity of the variations in '410' and '660' discontinuities topography. Also, we have generated direct difference curve plots for all stations for all three events in Appendix A.

2.2.2 Sensitivity of the S-wave to the Topography in the '410' and '660' discontinuities

For the horizontal transverse component seismograms we selected the following group of seismic phases taking into consideration that these phases interact with the mantle: Sdiff, SKS, SKKS, SKIKS, S660S, S410S, ScS660ScS, ScS410ScS, SS, SS660S, SS410S, SSS, ScSScs, SSSS and ScSScSScS. The theoretical ray paths for the seismic phases are illustrated in Figure 6.

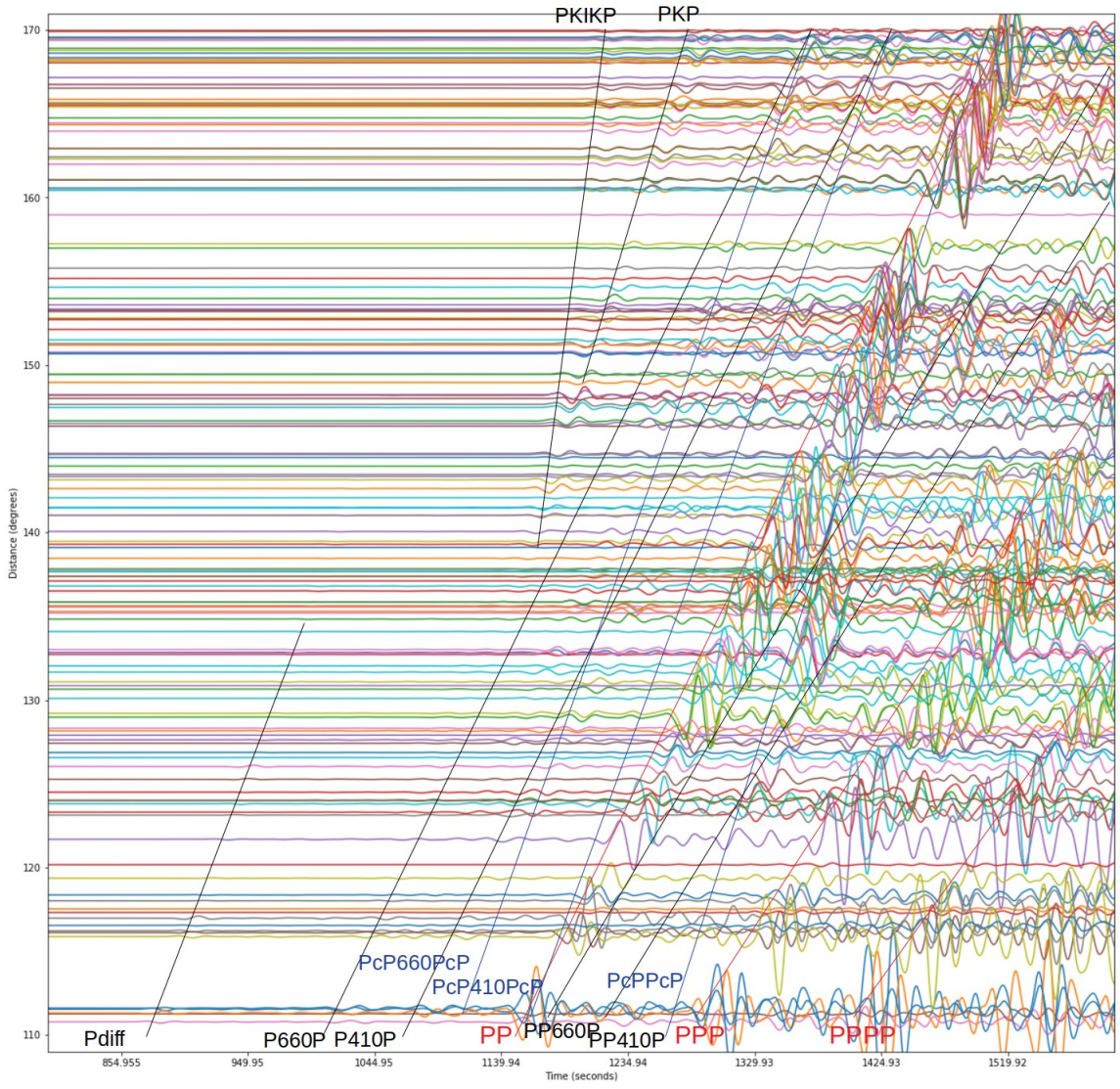

Figure 4: Amplitude Direct Difference (Δ1D) for all stations - Vertical Component (1D Elastic Model)

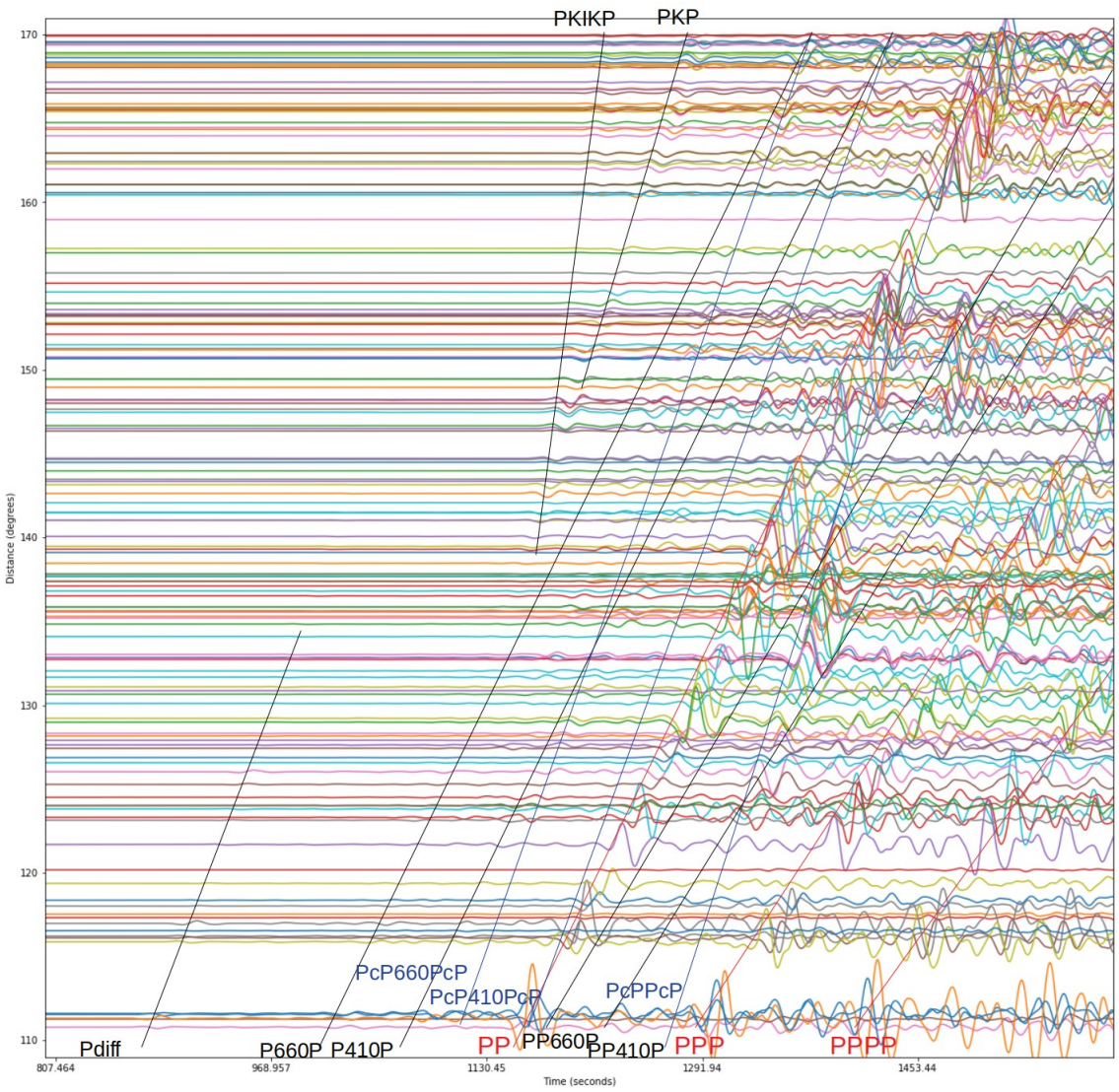

Figure 5: Amplitude Differences (Δ3D) for all stations Vertical Component (3D Model)

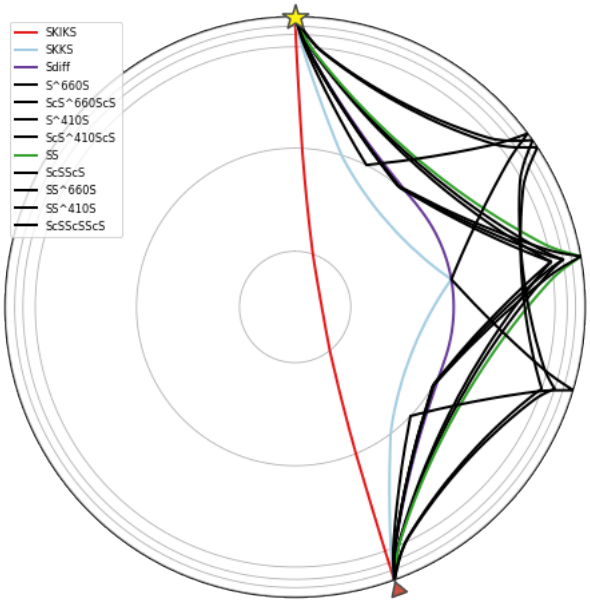

Figure 6: Raypaths of the Shear Wave seismic phases investigated

Phase	Arrival (seconds)	Δ1D	Δ3D	Sensitivity
PKIKP	1201.313	2.68e-04	8.45e-05	Low
PKP	1260.115	4.16e-04	3.29e-04	Moderate
P660P	1348.065	9.61e-04	5.27e-04	Moderate
PcP660PcP	1353.477	3.61e-04	2.02e-04	Low
P410P	1396.504	1.07e-04	1.02e-03	Moderate
PcP410PcP	1403.538	1.51e-04	5.33e-04	Low
PP	1486.512	1.93e-03	2.59e-03	High
PcPPcP	1495.665	2.71e-03	2.67e-03	High
PP660P	1595.697	5.49e-03	3.50e-03	High
PP410P	1636.390	1.86e-03	8.95e-04	Hgh
PPP	1718.273	1.52e-04	1.06e-03	Moderate
PPPP	1866.495	8.31e-04	4.78e-04	Moderate
PcPPcPPcP	1899.532	3.34e-03	9.15 e-03	High

Table 2: Normalised amplitude direct difference values for a station with epicentral distance 141.75° - Vertical Component (1D Elastic Model)

1D Elastic Model

Seismograms were generated using the 1D elastic model PREM. Two cases were created: one case without topographic anomalies in the '410' and '660' km discontinuities and one case with topographic anomalies. We evaluated the amplitude variations caused in the waveforms. In Figure 7 we observe an example of a pair of seismograms obtained for a station with epicentral distance 165.75°. The orange line corresponds to the seismogram with topography on the 410' and 660' discontinuities, whereas the blue line is the seismogram for the same earth model without topography on '410' and '660' discontinuities. The figure shows the arrivals for the body phases SKKS, S660S, S410S and SS in both seismograms.

To evaluate the differences created in the seismograms by the addition of topography variations in the '410' and '660' discontinuities we calculated the amplitude direct difference of both seismograms using Equation 1 in a window of 30 seconds after the theoretical traveltime arrival of each seismic phase. The results for the example station are found in Table 4 in the column Δ1D. The values calculated indicate that the highest difference in amplitude results for the arrivals corresponding to multiples, followed by the precursors (S660S and S410S) and core reverberations (ScS660ScS and ScS410ScS). The smaller amplitude differences are presented by the SKIKS and SKKS phases (phases that travel through the core). The same exercise was carried out for all the stations. In Figure 8, curves are presented, where differences calculated with Equation 1 are plotted for all the stations used in the simulations for the 1D elastic model simulations. Marked in lines are the theoretical arrivals of the seismic phases. As well as for the P-wave exercise, we assessed in a quantitative way variations by calculating the amplitude direct differences in a window of 30 seconds for each S-wave seismic phase evaluated for all stations.

3D Elastic Model

Using the same methodology as in the 1D cases we analyzed seismograms generated using the earth model S20RTS + CRUST2.0. We evaluated the variations caused in the waveforms by adding the topography in the 410' and 660' discontinuities by calculating the direct difference between the two waveforms using Equation 2 using a 30 seconds window after the theoretical traveltime arrivals for each seismic phase evaluated.

The results for the example station are found in Table 4 in the column Δ3D. In this table we can observe the behaviour of the sensitivity of the seismic phases for the 1D elastic model is preserved for the seismograms computed in the 3D elastic model. Also, as in the 1D case, amplitude direct difference curves were calculated between the seismograms pairs for all stations, presented in Figure 9. From the response of the waveforms observed for the 3D Elastic Model case we can observe that the behaviour seen in the 1D Elastic Model cases prevails (Figure 8).

Effect of event depth in S-wave seismic phases:

For the transverse component we also evaluated the responses caused by varying the depth of the event. Seismogram pairs produced for 1D and 3D elastic models with event depths of 20, 150 and 500 km were evaluated

Event Depth	Low Sensitivity	Moderate Sensitivity	High Sensitivity
20 km	Pdiff, P660P, PcP660PcP, P410P, PcP410PcP	PKIKP, PKP, PP410P, PP660P, PKKP, PKIKKIKP	PP, PPP, PPPP, PcPPcP, PcPPcPPcP
150 km	Pdiff, PKIKP, PKP, P660P, PcP660PcP, P410P, PcP660PcP	PP, PKKP, PKIKKIKP	PP, PP410P, PP660P, PPP, PPPP, PcPPcP, PcPPcPPcP
500 km	Pdiff, PKIKP, PKP, P660P, PcP660PcP, P410P, PcP410PcP	PKKP, PKIKKIKP	PP, PP660P, PP410P, PPP, PPPP, PcPPcP, PcPPcPPcP

Table 3: Classification of P-wave seismic phases according to sensitivity to variations in topography in '410' and '660' discontinuities

visually and quantitatively in the same manner as the P-wave seismic phases. In general it was observed that the behaviour of the sensitivity of the seismic phases to topography in the '410' and '660' discontinuities did not change. We summarized a classification of the sensitivity of the seismic phases in Table 5.

In Appendix A,plots are presented of the direct difference curves from the transverse component for all stations, for both 1D and 3D elastic models. Examining the plot for the 1D elastic model for the event of 20 km depth we can observe clearly the responses corresponding to the seismic phases Sdiff, S660S, S410S and SS the difference curves show amplitudes, indicating that these phases are sensitive to variations in the topography. The same is also true for the plots that belong to event depths 150 km and 500 km. However, we can also recognize for the deeper event plots the arrivals sSdiff and sSS. This phases are produced by waves leaving upward from the source. These seismic phases are also produced for the 20 km depth event but their arrivals are very close to the downward going waves, so they are not identified separately.

From the comparison of the difference curves for the simulations with event depths of 20 km, 150 km and 500 km we can observe that for both transverse and vertical component seismograms the seismic phases that are time shifted due to the topography of the '410' and '660' discontinuities do not vary.

2.3 Real Event Comparison with Synthetic Experiment

After the evaluation of the response of seismic phase in amplitude difference to topography of the '410' and '660' discontinuities, we proceeded to investigate the seismic phases sensitivity for the shear wave in a case using real waveforms. The goal with this experiment is to determine if we observe the same behaviour in seismic phases sensitivity as in the previous synthetic experiments.

A real event was chosen considering to have as good as possible spread of stations for the the epicentral distances from 110° to 170°, as well as a relevant quantity of stations. The event parameters are shown in Table 6. The real waveforms were obtained for 329 stations (Stations used are seen in Figure 10). The synthetic seismograms were generated for the same stations.

2.3.1 Traveltime difference

To assess the synthetic waveforms generated using spectral-elements modelling using `SPECFEM3D_GLOBE` using a background earth model plus topography in the '410' and '660' discontinuities with respect to real waveforms recorded by seismological stations we decided to measure cross-correlation traveltime difference in 50 seconds windows for each seismic phase with a timeshift of 20 seconds. The seismic phases evaluated are: Sdiff, S660S,

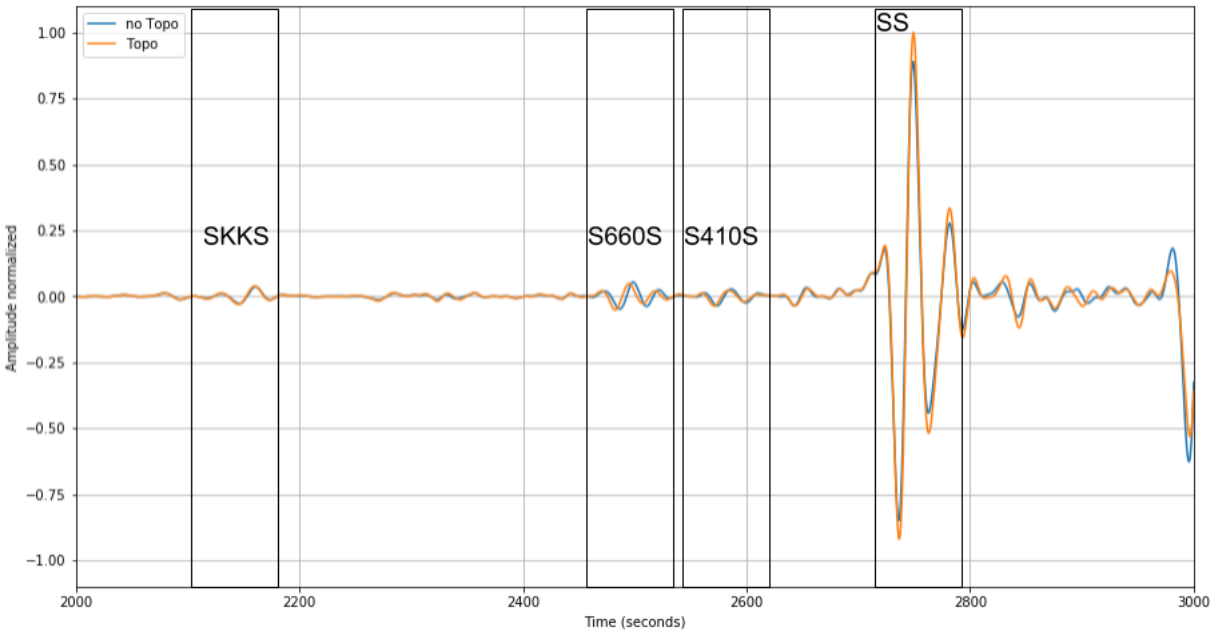

Figure 7: Transverse component seismograms for a station with epicentral distance 165.75° - 1D Elastic Model

S410S, ScS660ScS, ScS410ScS, SS, SS660S, SS410S, ScSScS, SSS, ScSScSScS and SSSS. This group of seismic phases was selected from the results of the synthetic experiments, where it was observed that these phases where classified between moderate and large sensitivity to variations in topography in the '410' and 660' discontinuities.

1D Elastic Model

For this case the synthetic seismograms were created using the 1D elastic model PREM + Topography in the '410' and '660' discontinuities. We compared the synthetic and real waveforms by cross-correlation, obtaining traveltime differences (δt) that correspond to the maximum value of the crosscorrelation function for a 50 seconds time window (See Equation 3).

$$\delta t = t_{phase}^{RealEarth} - t_{phase}^{PREM+Topo} \tag{3}$$

3D Elastic Model

For this case the synthetic seismograms were created using the 1D elastic model S20RTS + CRUST2.0 + Topography in the '410' and '660' discontinuities. We compared the synthetic and real waveforms by cross-correlation, obtaining traveltime differences (δt) that correspond to the maximum value of the cross-correlation function for a 50 seconds time window (See Equation 4).

$$\delta t = t_{phase}^{RealEarth} - t_{phase}^{S20RTS+Topo} \tag{4}$$

3 Results

We measured the traveltime differences for all the stations between the earth model waveforms and the real earth waveforms for both the 1D elastic model case and the 3D model case. The results are presented in histograms. For the case of a 1D elastic model the results can be seen in Figures 11, 12 and 13. For the case of a 3D elastic model the results can be seen in Figures 14, 15 and 16.

From the histograms presented in Figure 11 and 14 we can observe that the SS precursors S660S and S410S show sensitivity with a traveltime shift values of around 2-5 seconds, though the histogram for the SS precursors is very spread. We think this could be related to their weak amplitude, which results in difficulty to properly isolating them. Also, due to the effect of strong trade-off between shear velocity and topography in their time

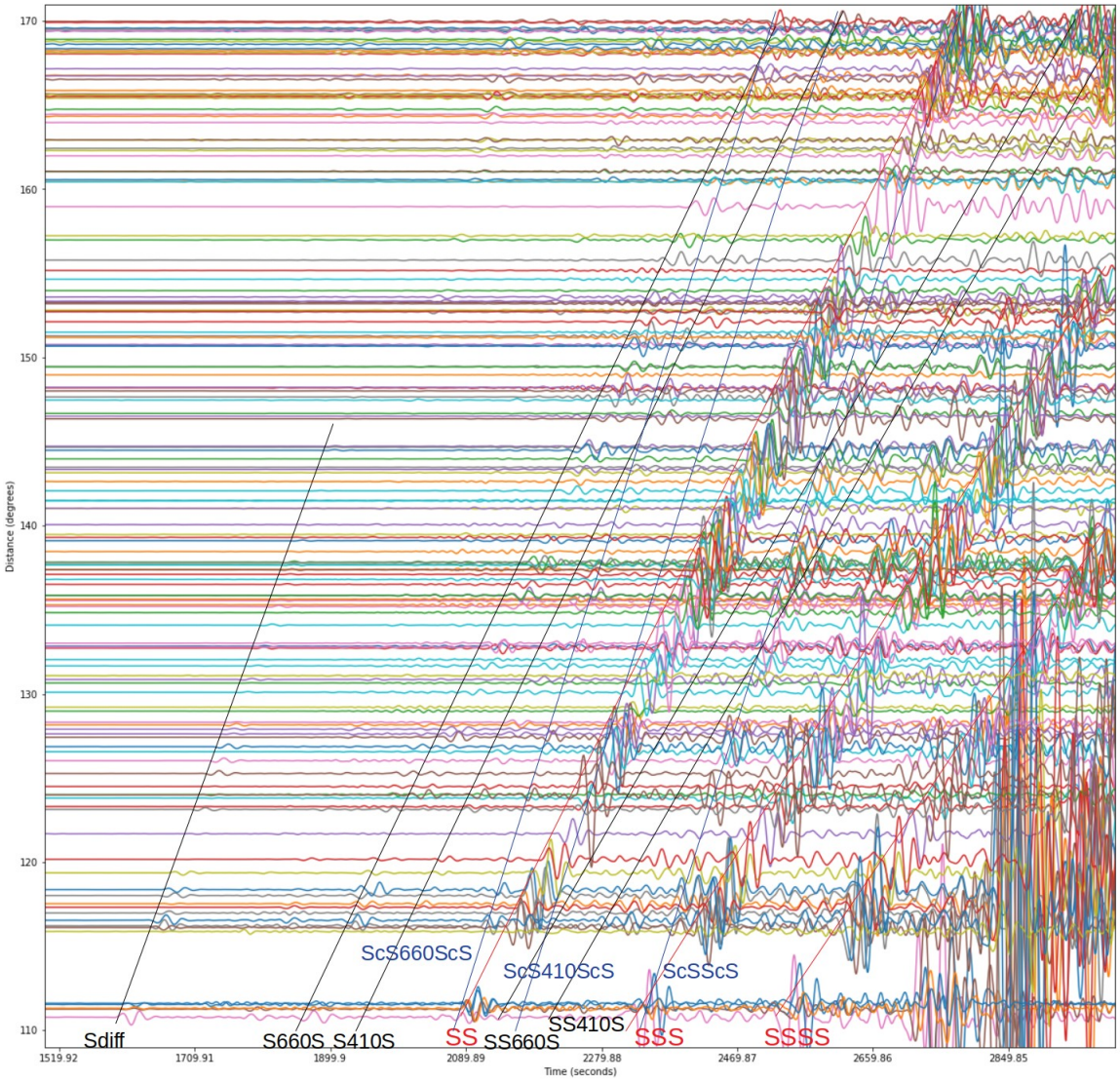

Figure 8: Amplitude direct difference (Δ1D) curves calculated for all stations. Marked in lines are the theoretical arrivals of the seismic phases in the epicentral distance range 110° to 170°

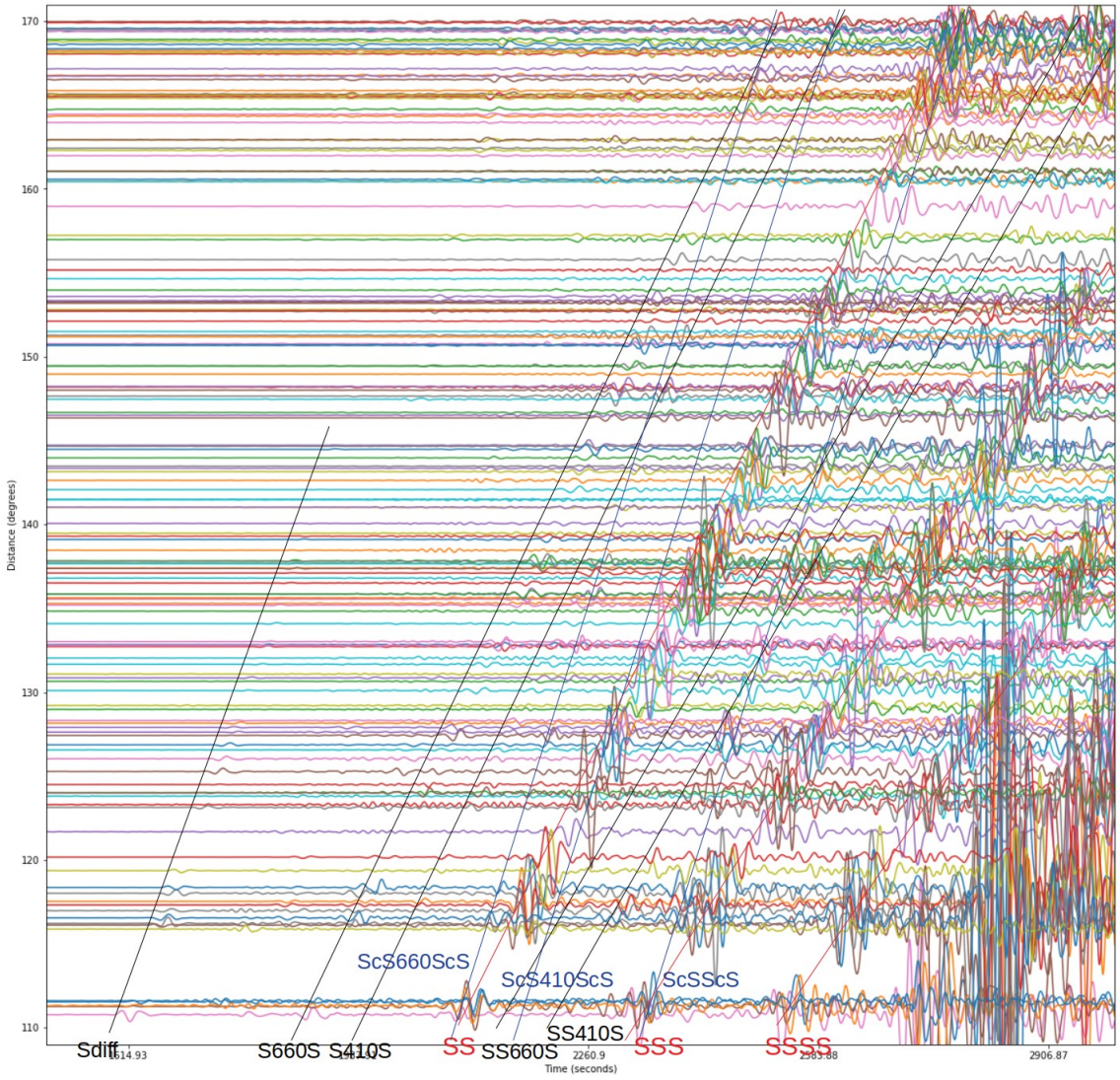

Figure 9: Differences calculated for all stations using the 3D Elastic Model. Marked in lines are the theoretical arrivals of the SS phase and the 410 and 660 precursors in the epicentral distance range 110 to 170.

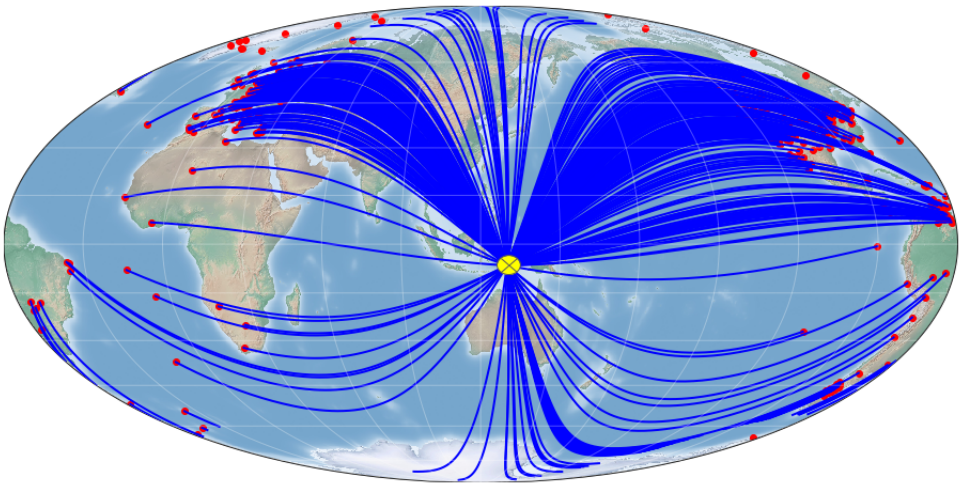

Figure 10: Stations distribution for real event. Epicenter: yellow circle. Stations: red circles. Great circle paths between event and stations: Blue lines

Phase	Arrival (seconds)	Δ 1D	Δ 3D	Sensitivity
SKIKS	1625.243	6.69-05	4.39e-05	Low
SKKS	1893.231	6.08e-05	1.31e-04	Low
S660S	2475.830	3.88e-03	1.69e-03	Moderate
ScS660ScS	2495.094	4.16e-03	1.57e-03	Moderate
S410S	2563.364	1.86e-03	1.16e-04	Moderate
ScS410ScS	2587.123	1.41e-03	4.51e-04	Moderate
SS	2725.433	9.88e-03	1.02e-02	High
ScSScS	2754.769	9.19e-03	3.63e-03	High
SS660S	2891.471	5.90e-03	7.01e-03	High
SS410S	2965.856	3.07e-03	4.39e-03	High
SSS	3168.361	1.07e-02	1.40e-02	High
SSSS	3374.954	1.73e-02	2.80e-02	High

Table 4: Normalised amplitude direct difference values for a station with epicentral distance 165.75° - Transverse Component (1D Elastic Model)

Event Depth	Low Sensitivity	Moderate Sensitivity	High Sensitivity
20 km	Sdiff, SKS, SKKS, SKIKS	S410S, S660S, ScS410ScS, ScS660ScS, SS410S, SS660S	ScSScS, SS, SSS, SSSS, ScSScSScS
150 km	SKS, SKKS, SKIKS	Sdiff, S410S, S660S, ScS410ScS, ScS660ScS	ScSScS, SS, SS410S, SS660S, SSS, SSSS, ScSScSScS
500 km	SKS, SKKS, SKIKS	Sdiff, S410S, S660S, ScS410ScS, ScS660ScS	ScSScS, SS, SS410S, SS660S, SSS, SSSS, ScSScSScS

Table 5: Sensitivity of seismic phases with depth. Transverse Component

windows [Koroni et al., 2017].

In the histograms shown in Figures 12 and 15 we can observe the traveltime shifts presented by the S multiples and SS precursors SS660S and SS410S. These phases present higher traveltime difference values than the S660S and S410S precursors. We infer that these values correspond to the addition of each interaction with the upper mantle discontinuities.

Additionally, in the histograms shown in Figures 13 and 16 we observe the results for the ScS core reverberations seismic phases. These phases show a very clear traveltime shift values of 14-18 seconds, for both 1D and 3D elastic models. For these seismic phases we consider as well that the high traveltime difference values they present correspond to long travelling paths interacting with many regions in the whole mantle.

4 Discussion

In the experiments comparing synthetic waveforms generated using the spectral-element method, we could observe sensitivity presented in a group of seismic phases, for both shear and compressional wave. The sensitivity was measured in terms of amplitude direct difference. Consequently we proposed a qualitative classification of the sensitivity of these seismic phases, which can be summarized as follows:

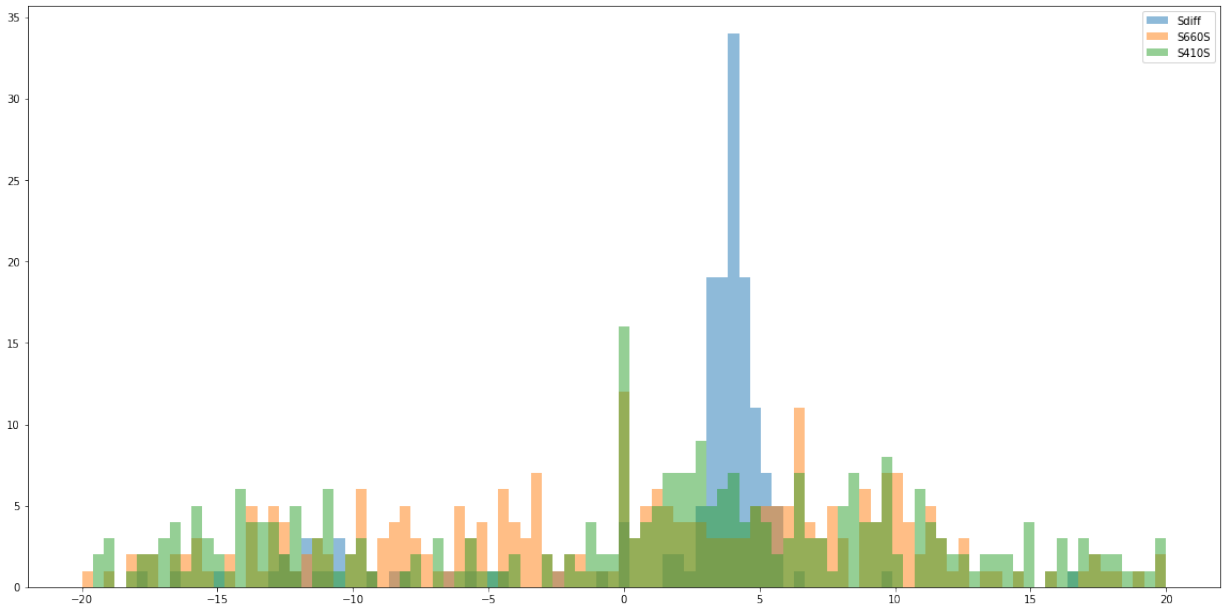

Figure 11: Traveltime difference for 1D elastic model - Seismic phases: Sdiff, S660S and S410S

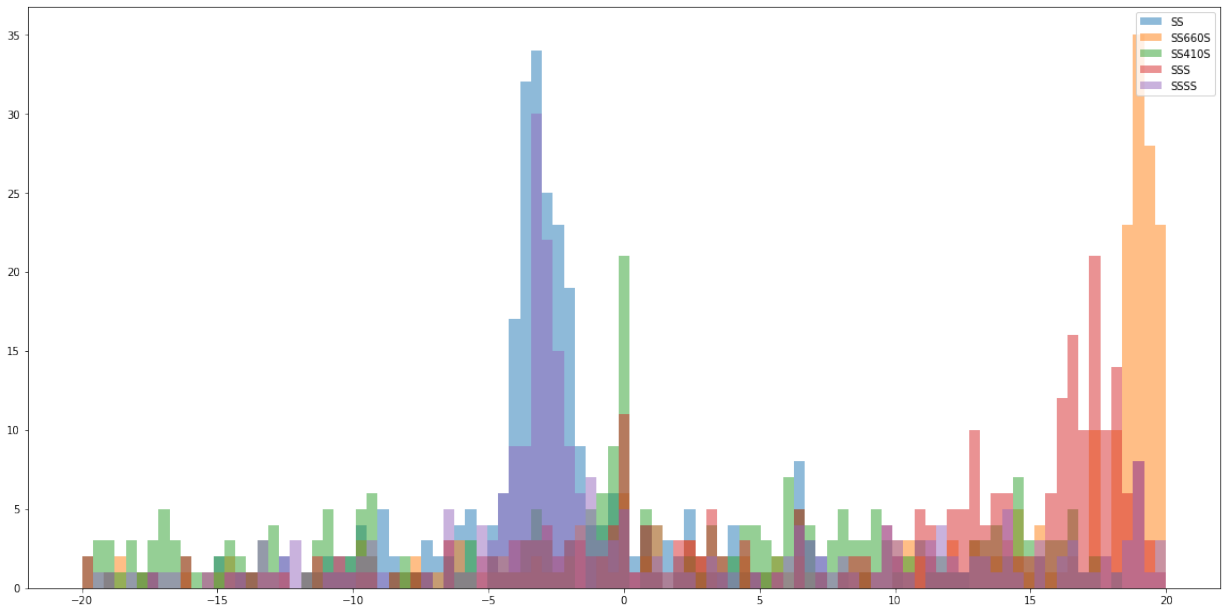

Figure 12: Traveltime difference for 1D elastic model - Seismic phases: SS, SS660S, SS410S, SSS and SSSS

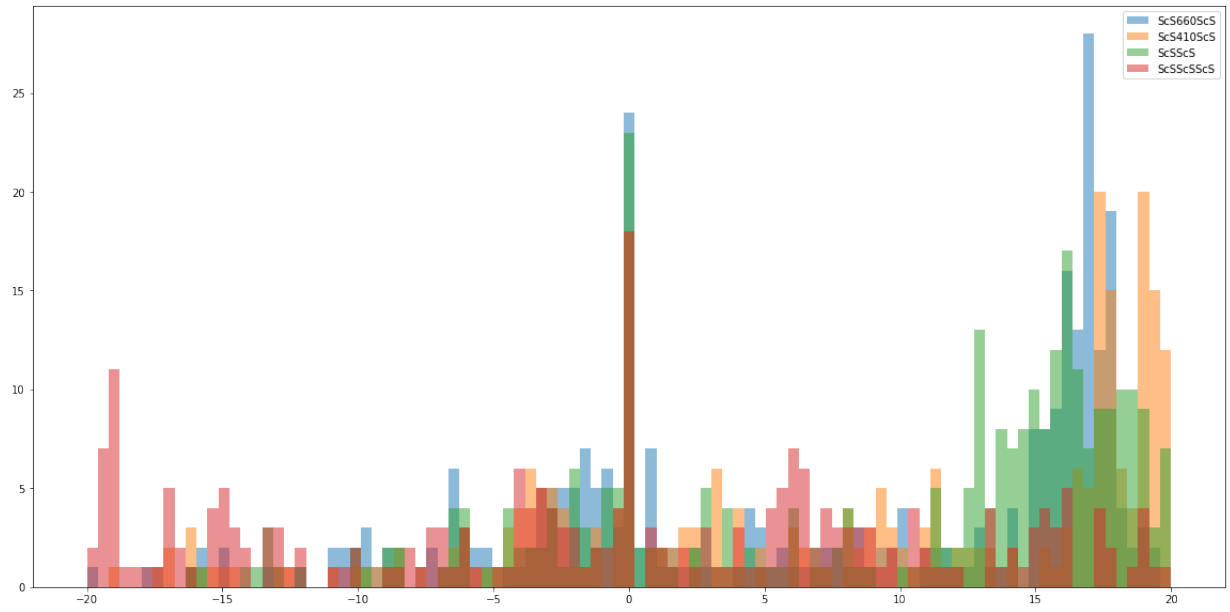

Figure 13: Traveltime difference for 1D elastic model - Seismic phases: ScS660ScS, ScS410ScS, ScSScS and ScSScSScS

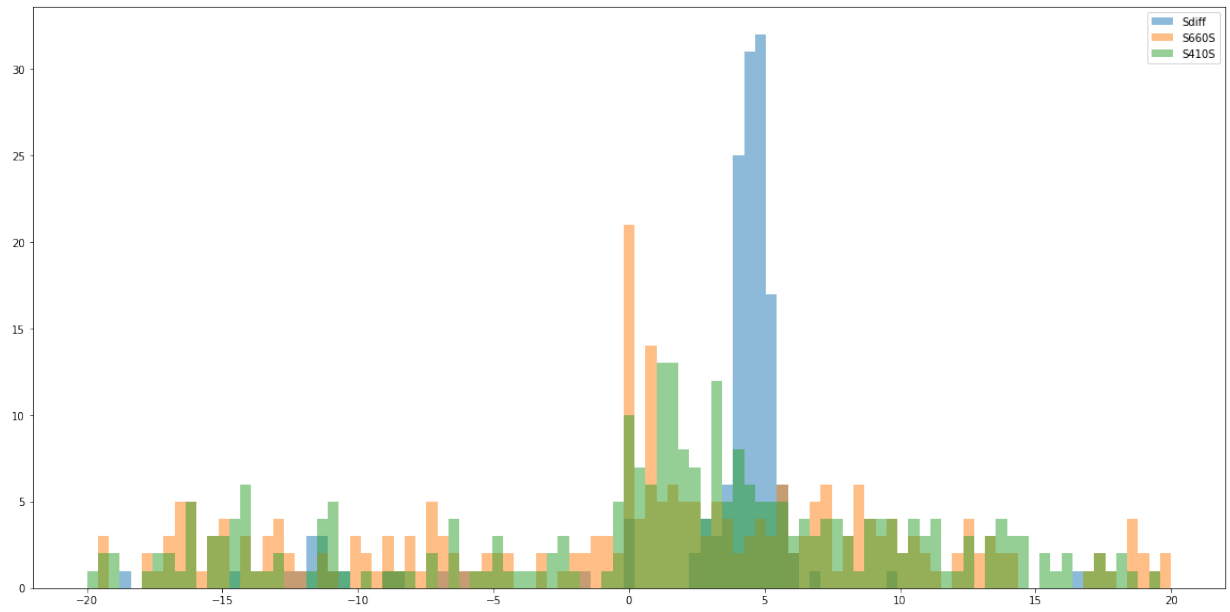

Figure 14: Traveltime difference for 3D elastic model - Seismic phases: Sdiff, S660S and S410S

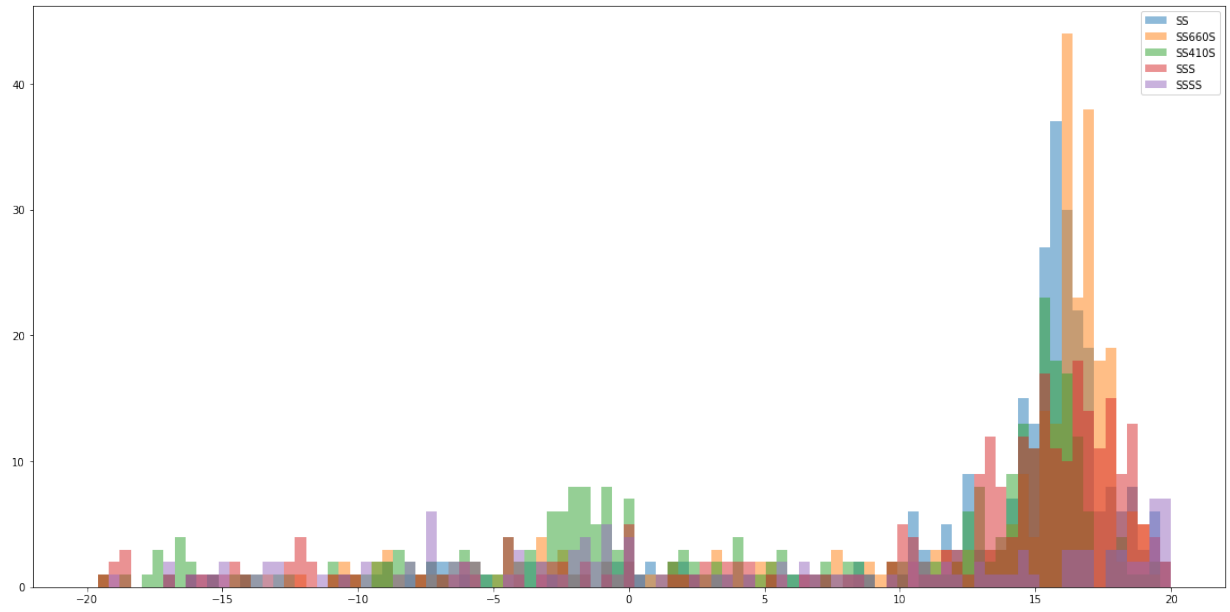

Figure 15: Traveltime difference for 3D elastic model - Seismic phases: SS, SS660S, SS410S, SSS and SSSS

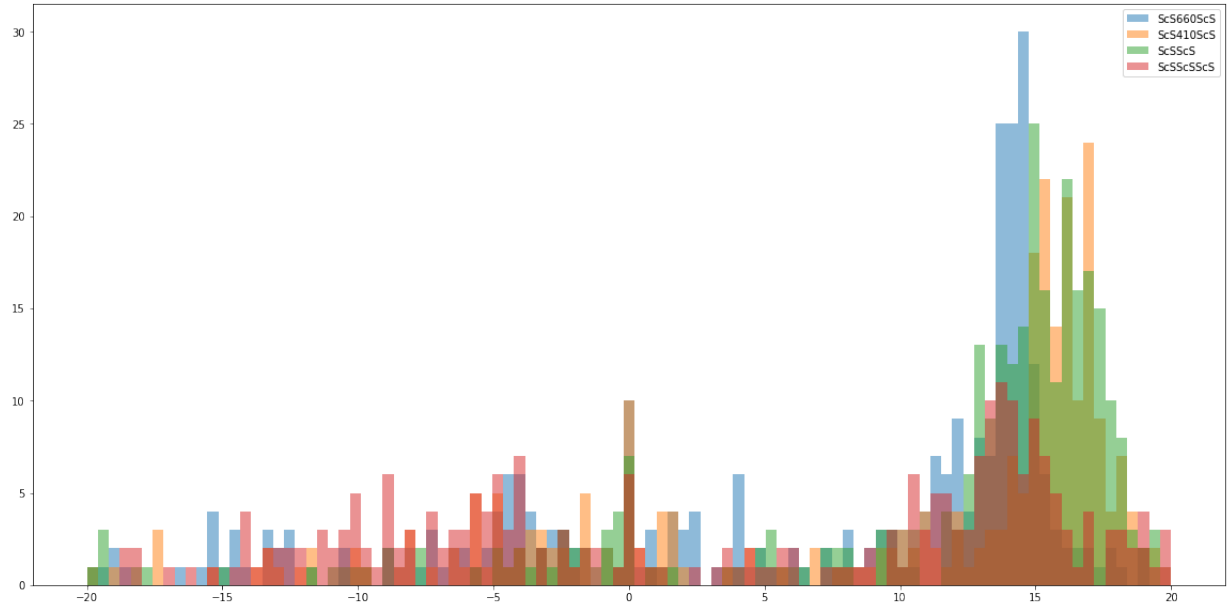

Figure 16: Traveltime difference for 3D elastic model - Seismic phases: ScS660ScS, ScS410ScS, ScSScS and ScSScSScS

Date / Time (UTC)	2005-03-02 10:42:09 UTC
Location	Banda Sea, Indonesia
Magnitude	MW 7.1
Latitude	6.5657° S
Longitude	129.8801° E
Depth	197.6 km

Table 6: Event Parameters

1. For compressional wave seismic phases, the highest sensitivity is presented by P-wave multiples and core reverberations (PcP). With the same reference, core phases (PKKP and PKIKKIKP) would have moderate sensitivity and PP precursors would have the lowest sensitivity (we consider this results to be reliable, since the low effect of topography on the '410' and '660' for the PP precursors is also referenced in literature [Koroni et al., 2019]).

2. For shear wave the most sensitive waves to variations in topography to the '410' and '660' discontinuities, are S-wave multiples and core reverberations (ScS). In the same manner, Sdiff and SS precursors would have moderate sensitivity and core phases would have the lowest sensitivity.

We can find numerous examples in literature for some of the seismic phases evaluated to be used in the investigation of the upper mantle discontinuities. The most commonly used are the SS precursors (S660S and S410S), which although by nature contain low amplitudes, their sensitivity to topography in the upper mantle discontinuities has been affirmed by multiple studies, where we can reference the following: [Rychert et al., 2014], [Rychert et al., 2012], [Schmerr and Garnero, 2006], [Deuss, 2009], [Deuss and Woodhouse, 2002], [Shearer, 1993], [Flanagan and M. Shearer, 1998] and [Koroni and Trampert, 2016].

Likewise, the ScS core reverberations have also been used in previous research studies to evaluate the topography of the upper mantle discontinuities. Some examples in the literature can be found in [Rychert et al., 2012], [Wang et al., 2017], [Tono et al., 2005] and [Revenaugh and Jordan, 1991].

In regard to the compressional wave, a number of studies also have approached the upper mantle discontinuities using the PP precursors. Some examples in the literature can be found in [Bentham et al., 2017], [Deuss, 2009], [Koroni et al., 2019], [Lessing et al., 2015] and [Estabrook and Kind, 1996].

Some of the seismic phases evaluated have not been used previously in the investigation of the structure of the '410' and '660' upper mantle discontinuities, although in our synthetic experiments we can observe there are clear variations in their arrivals caused by the addition of topography. Thus, they should be incorporated in a full waveform inversion scheme since they are evidently informative about discontinuity topography.

Evaluating transverse component waveforms recorded for a real event with respect to synthetic waveforms generated with 1D and 3D elastic models using as a reference travel time delay of the response of seismic phases in the waveforms we can make the following remarks: we consider that the the seismic phases Sdiff, S660S and S410S precursors, and S-wave multiples have a moderate sensitivity. The core reverberations ScS have a higher sensitivity.

5 Conclusions

Our analysis shows that using waveforms generated from spectral-element modelling we can correctly assess the sensitivity of seismic phases to the topography in the upper mantle discontinuities. We were able to evaluate the sensitivity of seismic phases to the variations in topography of the '410' and '660' discontinuities of the upper mantle by two different methods (amplitude direct difference of synthetic waveforms and cross-correlation traveltime difference of synthetic and real waveforms), which provided us with similar behaviours for the seismic phases evaluated in the shear wave.

Travel time delay values obtained comparing synthetic waveforms generated using both 1D and 3D elastic models with real waveforms indicated high sensitivity for the core reverberations seismic phases, but also showed sensitivity for SS multiples and SS precursors. This behaviour is very similar to the sensitivities obtained by

calculating amplitudes direct difference of synthetic waveforms.

We consider that the seismic phases classified as moderate and high sensitivity for both the shear and compressional wave can be further used for the full-waveform inversion of the upper mantle discontinuities.

6 Recommendations

It is essential to further evaluate the interaction and behaviour of these seismic phases regarding the upper mantle discontinuities. Consequently, it is recommended to use the adjoint method to investigate the sensitivity kernels for both 1D and 3D elastic models, to additionally develop more knowledge that contributes to a more efficient incorporation of the observable traveltime of these body wave phases in a full-waveform inversion.

References

[Bassin et al., 2000] Bassin, C., Laske, G., and Masters, G. (2000). The current limits of resolution for surface wave tomography in North America. *EOS*, 81:F897.

[Bentham et al., 2017] Bentham, H., Rost, S., and Thorne, M. (2017). Fine-scale structure of the mid-mantle characterised by global stacks of pp precursors. *Earth and Planetary Science Letters*, 472:164 – 173.

[C. Schmerr et al., 2010] C. Schmerr, N., Chen, C., and Sun, D. (2010). Probing mantle transition zone heterogeneity with topside reflected sh seismic energy (invited). *AGU Fall Meeting Abstracts*.

[Cottaar and Deuss, 2015] Cottaar, S. and Deuss, A. (2015). Large-scale mantle discontinuity topography beneath europe: Signature of akimotoite in subducting slabs. *Journal of Geophysical Research: Solid Earth*, 121:n/a–n/a.

[Crotwell et al., 1999] Crotwell, H. P., Owens, T. J., and Ritsema, J. (1999). The taup toolkit: Flexible seismic travel-time and ray-path utilities. *Seismological Research Letters*, 70(2):154–160.

[Deuss, 2009] Deuss, A. (2009). Global observations of mantle discontinuities using *SS* and *PP* precursors. *Surv. Geophysics*, 30:301–326.

[Deuss and Woodhouse, 2002] Deuss, A. and Woodhouse, J. H. (2002). A systematic search for mantle discontinuities using ss-precursors. *Geophysical Research Letters*, 29(8):90–1–90–4.

[Dziewonski and Anderson, 1981] Dziewonski, A. M. and Anderson, D. L. (1981). Preliminary reference earth model. *Physics of the Earth and Planetary Interiors*, 25(4):297 – 356.

[Estabrook and Kind, 1996] Estabrook, C. H. and Kind, R. (1996). The nature of the 660-kilometer upper-mantle seismic discontinuity from precursors to the pp phase. 274(5290):1179–1182.

[Flanagan and M. Shearer, 1998] Flanagan, M. and M. Shearer, P. (1998). Global mapping of topography on transition zone velocity discontinuities by stacking ss precursors. *Journal of Geophysical Research*, 103:2673–2692.

[Helffrich, 2000] Helffrich, G. (2000). Topography of the transition zone seismic discontinuities. *Reviews of Geophysics*, 38(1):141–158.

[Hirose, 2002] Hirose, K. (2002). Phase transitions in pyrolitic mantle around 670-km depth: Implications for upwelling of plumes from the lower mantle. *Journal of Geophysical Research: Solid Earth*, 107(B4):ECV 3–1–ECV 3–13.

[Katsura et al., 2004] Katsura, T., Yamada, H., Nishikawa, O., Song, M., Kubo, A., Shinmei, T., Yokoshi, S., Aizawa, Y., Yoshino, T., Walter, M. J., Ito, E., and Funakoshi, K.-i. (2004). Olivine-wadsleyite transition in the system (mg,fe)2sio4. *Journal of Geophysical Research: Solid Earth*, 109(B2).

[Komatitsch and Tromp, 1999] Komatitsch, D. and Tromp, J. (1999). Introduction to the spectral element method for three-dimensional seismic wave propagation. *Geophysical Journal International*, 139(3):806–822.

[Komatitsch and Tromp, 2002a] Komatitsch, D. and Tromp, J. (2002a). Spectral-element simulations of global seismic wave propagationI. Validation. *Geophysical Journal International*, 149(2):390–412.

[Komatitsch and Tromp, 2002b] Komatitsch, D. and Tromp, J. (2002b). Spectral-element simulations of global seismic wave propagationii. three-dimensional models, oceans, rotation and self-gravitation. *Geophysical Journal International*, 150(1):303–318.

[Komatitsch and Vilotte, 1998] Komatitsch, D. and Vilotte, J.-P. (1998). The spectral element method: an efficient tool to simulate the seismic response of 2d and 3d geological structures. *Bulletin of the Seismological Society of America*, 88:368–392.

[Koroni et al., 2017] Koroni, M., Bozdağ, E., Paulssen, H., and Trampert, J. (2017). Sensitivity analysis of seismic waveforms to upper-mantle discontinuities using the adjoint method. *Geophys. J. Int.*, 210:1965–1980.

[Koroni et al., 2019] Koroni, M., Paulssen, H., and Trampert, J. (2019). Sensitivity kernels of pp precursor traveltimes and their limitations for imaging topography of discontinuities. *Geophysical Research Letters*, 46(2):698–707.

[Koroni and Trampert, 2016] Koroni, M. and Trampert, J. (2016). The effect of topography of upper mantle discontinuities on *SS* precursors. *Geophys. J. Int.*, 204:667–681.

[Lessing et al., 2015] Lessing, S., Thomas, C., Saki, M., Schmerr, N., and Vanacore, E. (2015). On the difficulties of detecting PP precursors. *Geophysical Journal International*, 201(3):1666–1681.

[Meier et al., 2009] Meier, U., Trampert, J., and Curtis, A. (2009). Global variations of temperature and water content in the mantle transition zone from higher mode surface waves. *Earth and Planetary Science Letters*, 282(1-4):91–101.

[Revenaugh and Jordan, 1991] Revenaugh, J. and Jordan, T. (1991). Mantle layering from scs reverberations 3. the upper mantle. *Journal of Geophysical Research D: Atmospheres*, 96(B12).

[Ritsema et al., 1999] Ritsema, J., Heijst, H. J. v., and Woodhouse, J. H. (1999). Complex shear wave velocity structure imaged beneath africa and iceland. *Science*, 286(5446):1925–1928.

[Rychert et al., 2014] Rychert, C., Harmon, N., and Schmerr, N. (2014). Synthetic waveform modelling of ss precursors from anisotropic upper-mantle discontinuities. *Geophysical Journal International*, 196:3–.

[Rychert et al., 2012] Rychert, C. A., Schmerr, N., and Harmon, N. (2012). The pacific lithosphere-asthenosphere boundary: Seismic imaging and anisotropic constraints from ss waveforms. *Geochemistry, Geophysics, Geosystems*, 13(9).

[Schmerr and Garnero, 2006] Schmerr, N. and Garnero, E. (2006). Investigation of upper mantle discontinuity structure beneath the central pacific using ss precursors. *Journal of Geophysical Research: Solid Earth*, 111(B8).

[Shearer, 1991] Shearer, P. M. (1991). Constraints on upper mantle discontinuities from observations of long-period reflected and converted phases. *Journal of Geophysical Research*, 96:147–18.

[Shearer, 1993] Shearer, P. M. (1993). Global mapping of upper mantle reflectors from long-period ss precursors. *Geophysical Journal International*, 115(3):878–904.

[Tono et al., 2005] Tono, Y., Kunugi, T., Fukao, Y., Tsuboi, S., Kanjo, K., and Kasahara, K. (2005). Mapping of the 410-and 660-km discontinuities beneath the japanese islands. *Journal of Geophysical Research*, 110.

[Vasco and Johnson, 1998] Vasco, D. W. and Johnson, L. R. (1998). Whole earth structure estimated from seismic arrival times. *Journal of Geophysical Research: Solid Earth*, 103(B2):2633–2671.

[Vinnik, 1977] Vinnik, L. (1977). Detection of waves converted from p to sv in the mantle. *Physics of the Earth and Planetary Interiors*, 15(1):39 – 45.

[Vinnik, 2011] Vinnik, L. P. (2011). *Seismic Discontinuities in the Transition Zone*, pages 1102–1107. Springer Netherlands.

[Wang et al., 2017] Wang, X., Li, J., and Chen, Q.-F. (2017). Topography of the 410 km and 660 km discontinuities beneath the japan sea and adjacent regions by analysis of multiple-scs waves: Upper mantle structure beneath japan sea. *Journal of Geophysical Research: Solid Earth*, 122.

[Ward, 1978] Ward, S. N. (1978). Long-period reflected and converted upper-mantle phases. *Bulletin of the Seismological Society of America*, 68(1):133–153.

A Appendix 1

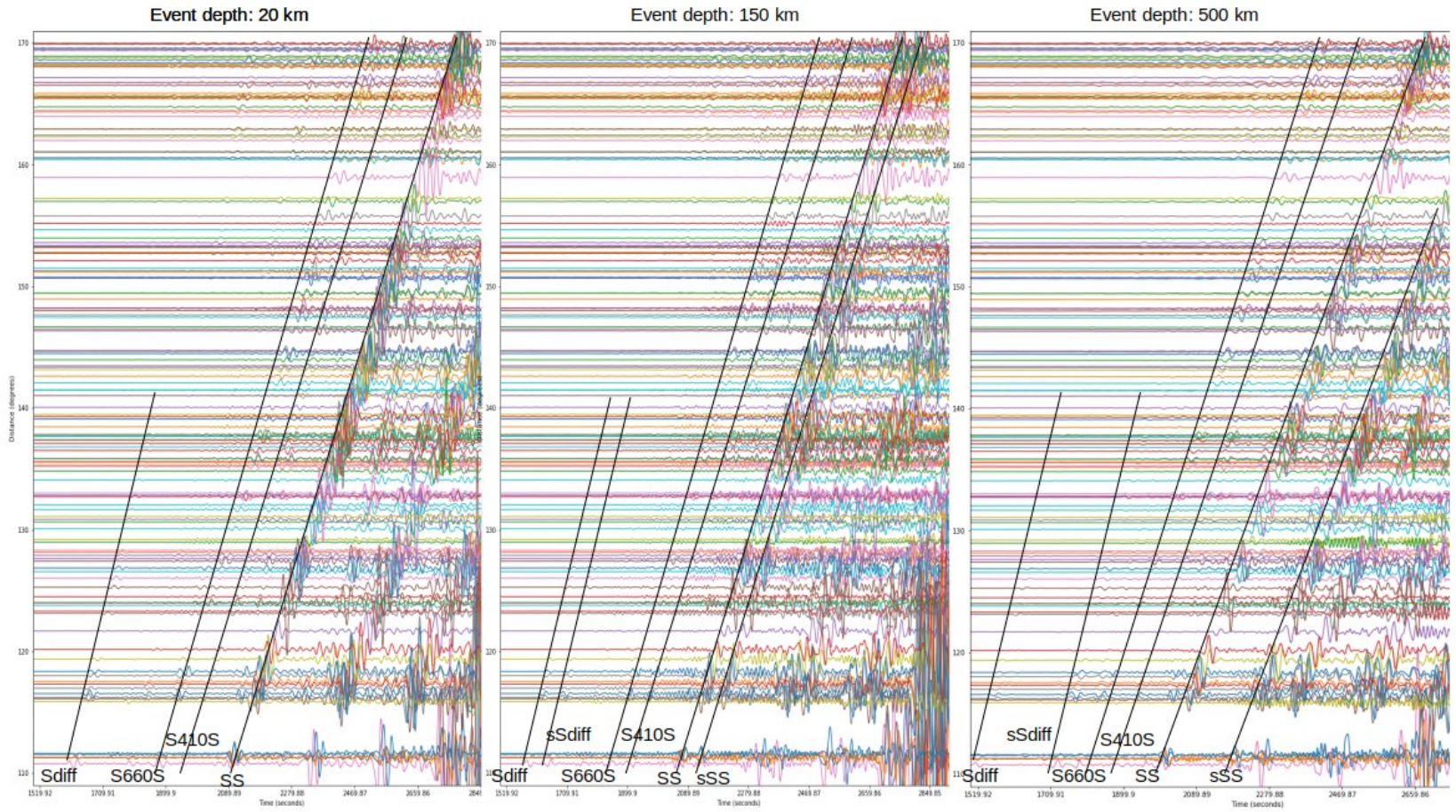

Figure 17: Amplitude Differences for all stations (Transverse component - 1D Elastic Model). Left: Event 20 km depth, Middle: Event 150 km depth, Right: Event 500 km depth.

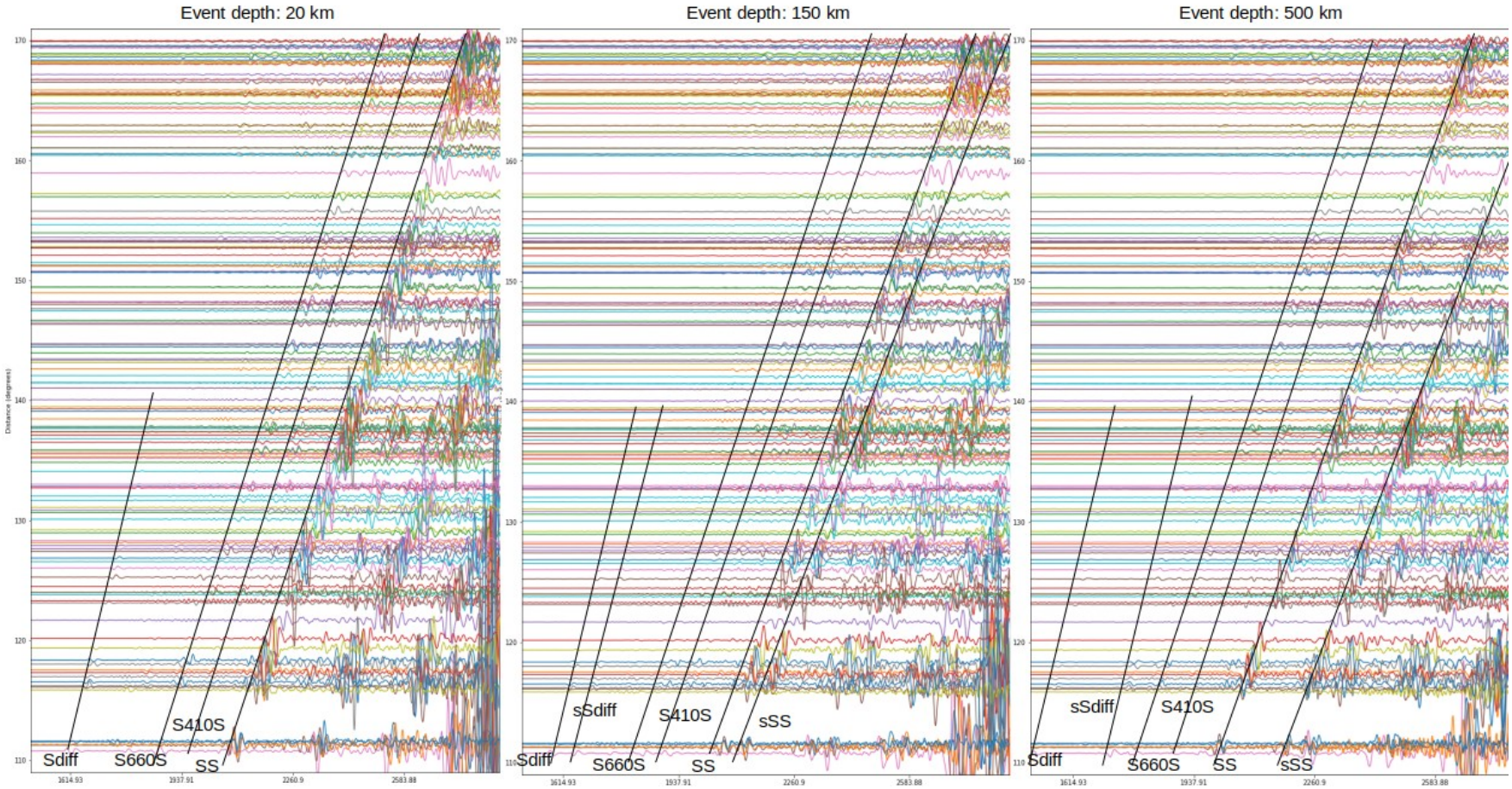

Figure 18: Amplitude Differences for all stations (Transverse component - 3D Elastic Model). Left: Event 20 km depth, Middle: Event 150 km depth, Right: Event 500 km depth.

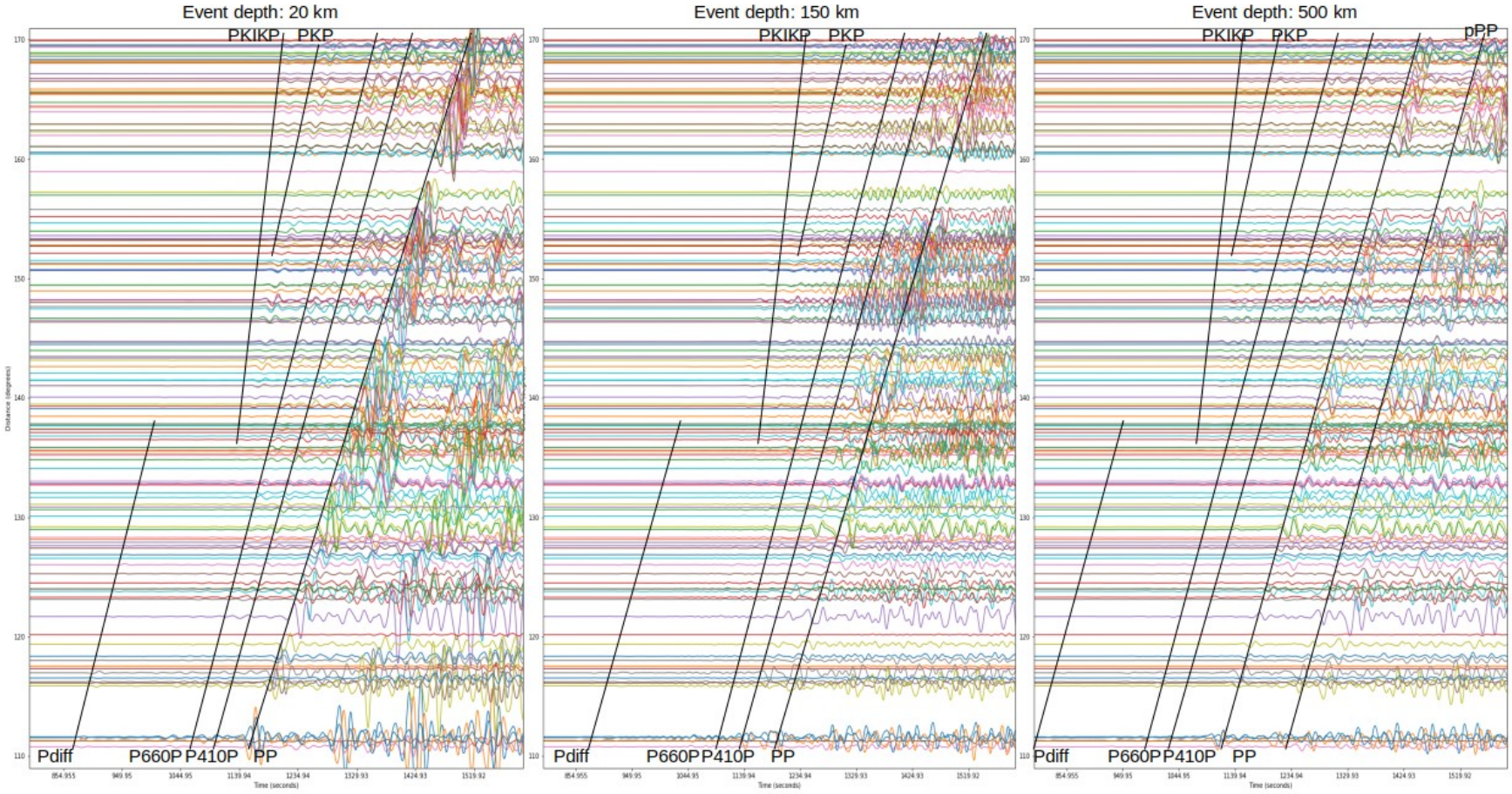

Figure 19: Amplitude Differences for all stations (Vertical component - 1D Elastic Model). Left: Event 20 km depth, Middle: Event 150 km depth, Right: Event 500 km depth.

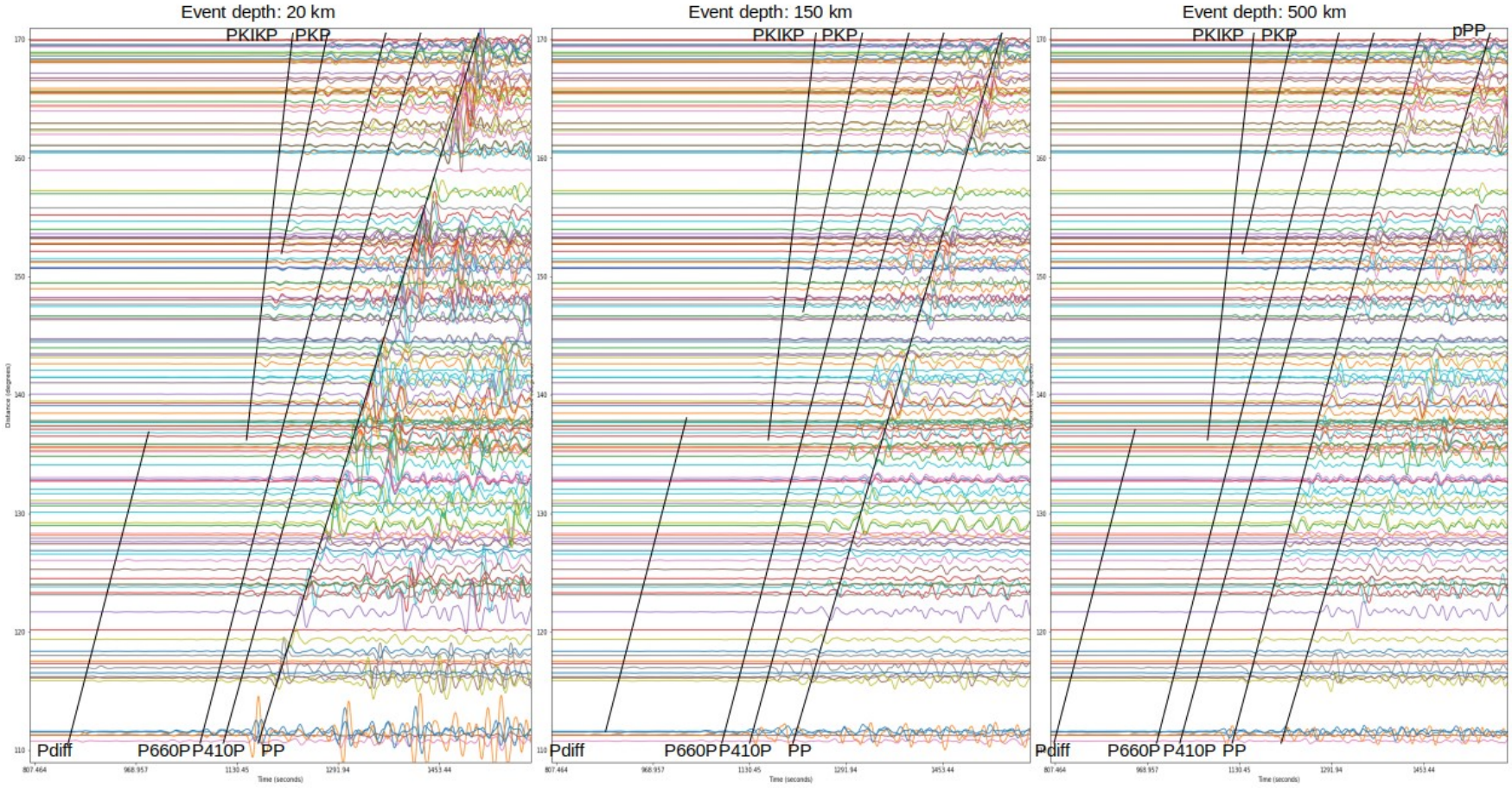

Figure 20: Amplitude Differences for all stations (Vertical component - 3D Elastic Model). Left: Event 20 km depth, Middle: Event 150 km depth, Right: Event 500 km depth.